The Performance Analysis of Tactical and Navigation Grade Land Inertial Navigation Systems Aided with Hypothetical Measurements

Lisan Ozan Yaman
Roketsan Missile Industries Inc.
Kemalpasa Mahallesi Sehit Yuzbasi Adem Kutlu Sokak No:21 06780 Elmadag/Ankara
TURKEY

ozan.yaman@roketsan.com.tr

ABSTRACT

Inertial Navigation System (INS) and inertial sensors are generally fundamental means of navigation for most majority of contemporary civil and military applications. Since INS is based on continuous integration of inertial sensors data, various type of measurements error built-in inertial sensors lead unbounded positioning error in time. This is the most fundamental reason that requires aiding INS with external navigation equipment such as Global Navigation Satellite System (GNSS) receiver. Although INS is extensively blended with GNSS receiver for most majority of practical applications, in such operation critical areas including urban/mountainous regions and intentional/nonintentional GNSS signal degraded environments, hypothetical measurements such as Zero Velocity Update (ZUPT), Zero Angular Rate Update (ZARUPT) and non-holonomic constraints (NHCs) are significant measurement assets to aid pure land inertial navigation system. Land inertial navigation systems benefit from ZUPT and ZARUPT aiding in static conditions whereas NHCs aiding improve navigation performance during platform motion states. Thus, hypothetical measurements aforementioned can be used in a complementary manner.

This paper closely examines the performance of both tactical and navigation grade inertial navigation system aided with the hypothetical measurements that can be applicable for land platforms. First, rigorous Monte-Carlo simulation analysis is carried out to obtain performance statistics for both tactical and navigation grades of inertial navigation systems. The Monte-Carlo simulation is developed for analysing horizontal position performance of aided INS with the simulated trajectories. According to each simulation set, the land platform initializes its navigation system with alignment phase and then the land vehicle undergoes a one hour constant speed cruise mission with a heading change trajectory that is based on constant heading change rate. Simulation studies indicate that as long as vehicle follows a non-straight path, the horizontal positioning performance of pure inertial navigation system is improved with exponential characteristics which is directly correlated to changes in platform heading angle. Later on, simulation studies are followed by experimental field tests via instrumented land vehicle equipped with well-known Inertial Measurement Units (IMU) called HG1700 and ISA-100C. The field navigation survey tests are carried out for five different trajectories with various distances and heading angle profiles. The test results indicate that better than 170 meters/hour (0.25% of travelled distance) horizontal positioning accuracy can be achievable with ISA-100C IMU while 500 meters/hour (0.75% of travelled distance) performance level is obtained with HG 1700. Both of the simulation analysis and experimental field tests verify that pure land inertial navigation systems can gain substantial amount of positioning performance by the aid of hypothetical measurements in algorithmic way without requiring any external hardware or equipment as long as the platform follow non-straight trajectory. The results obtained throughout this study prove that hypothetical measurements have a valuable potential to increase performance and robustness of inertial navigation systems during GNSS signal gaps and even signal denied environments.

1.0 INTRODUCTION

Today like many other aerial and naval navigation solutions, Inertial Navigation System (INS), especially Global Navigation Satellite System (GNSS) receiver integrated INS, is commonly fundamental technique for land platform navigation regardless of civil or military applications. Depending upon the enabling technologies and manufacturing procedures, inertial sensors contain different types of systematic and stochastic errors. Since the inertial navigation system solution depends on integration of both accelerometers and gyroscopes, INS navigation outputs suffers from unbounded error growth. Although inertial navigation system is immune to any external interference due to its self-contained operational feature, it should be supported with some sort of navigation aiding mechanisms or external navigation aiding hardware to limit the error growth. The GNSS receiver is the most common option as a navigation aiding sensor for almost all kind of applications including land platforms as well. When the operational scenario of the land vehicle equipped with GNSS receiver is concerned, there is a possibility of signal blockage in operation critical areas including urban/mountainous regions and GNSS signal degraded environments. Although there are various sources of navigation aiding such as doppler radar, odometer other than GNSS receiver available in the field, they still require utilization of external hardware. On the other hand, hypothetical measurements such as Zero Velocity Update (ZUPT), Zero Angular Rate Update (ZARUPT), Non-Holonomic Constraints (NHCs) are significant measurement asset to aid pure land inertial navigation system without the requirement of any external hardware. In this study, the aforementioned three hypothetical measurements are analysed for aiding pure inertial navigation systems.

Due to the nature of land vehicle application, the stationarity information and constrained motion that the land platform has to follow on the road can be used as valuable sources of navigation aiding information. Today, nearly all of the commercialized land inertial navigation systems contain built-in ZUPT feature which exploit the zero translational velocity information, either automatically or manually. However, ZUPT is not the only way of hypothetical measurements that can be applicable for land platforms' navigation mission. Similar to ZUPT case, ZARUPT or integrated ZARUPT can also be used for aiding inertial navigation system when the platform is in stationary phase. Moreover, NHCs measurement is very powerful source of velocity information when the platform is in motion. Therefore, both of the mentioned hypothetical measurements can aid the pure inertial navigation system in complementary manner. This paper closely examines the performance of the pure inertial navigation system aided with the hypothetical measurements mentioned above. Throughout this paper, theoretical work is carried out for tactical and navigation grade inertial navigation systems whereas the experimental work is done with high noise tactical and near navigation grade inertial navigation systems.

This paper is organized as follows. In the second chapter, algorithm structure and mathematical formulation of the estimation filter is given. Next chapter contains the details related to the idea of improving the robustness of the estimation filter. Chapter four and five highlight detailed analysis carried out in simulation and experimental environment. Finally, the conclusion part takes place to sum up the aforementioned studies.

2.0 ALGORITHM STRUCTURE & ESTIMATION FILTER MATHEMATICAL MODEL

The developed algorithm is based on well-known INS mechanization formulation and error state Extended Kalman Filter (EKF) structure. The functional flow-chart given below illustrates the working principles of the algorithm. The estimation filter exploits the hypothetical measurements when they are valid and suitable to use in order to estimate both inertial sensor and inertial navigation system errors. Validity control is explained in the part named "Robust Estimator" in a detailed manner.

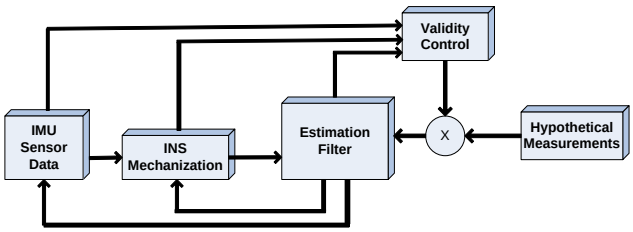

Figure 2-1: Algorithm functional flow chart

In this study, local navigation frame navigation equations with North-East-Down (NED) components based resolution frame is used as navigation mechanization. The details of inertial navigation system equations can be found in [1], [2], [3] and [4].

2.1 Notation

Throughout the study, the notation set given in Table 2-1 is extensively used.

Symbol	Definition	Symbol	Definition
$\vec{r}_{a/b}$	The position vector of the center point of the frame a with respect to the center point of the frame b. The vector $\vec{r}_{a/b}$ can be represented as $\vec{r}_{ba}$ and this notation is valid for all of the vector quantities.	$\tilde{\bar{x}}^c_{a/b}$	The error perturbed form of the column matrix $\bar{x}^c_{a/b}$. $\tilde{\bar{x}}^c_{a/b}=\bar{x}^c_{a/b}+\delta\bar{x}^c_{a/b}$
$\vec{v}_{a/b}$	The velocity vector of the center point of the frame a with respect to the center point of the frame b.	$ssm(\bar{x}^c_{a/b})$	The skew symmetric matrix form of the column matrix $\bar{x}^c_{a/b}$ $ssm(\bar{x}^c_{a/b})=\begin{bmatrix} 0 & -\bar{x}^c_{a/b}(3) & \bar{x}^c_{a/b}(2) \\ \bar{x}^c_{a/b}(3) & 0 & -\bar{x}^c_{a/b}(1) \\ -\bar{x}^c_{a/b}(2) & \bar{x}^c_{a/b}(1) & 0 \end{bmatrix}$
$\vec{a}_{a/b}$	The acceleration vector of the center point of the frame a with respect to the center point of the frame b.	$0_{3x3}, I_{3x3}$	Three by three zero and identity matrix respectively.
$D_a\{\ \}$	Derivative operator which applies time derivative with respect to the frame a.	η, w	The measurement and system noise symbols for the Kalman Filter application and they are modelled as white noise
δ	The error symbol.	σ	The standard deviation symbol or rms value uncertainty in the represented signal if it has a zero mean
$\bar{x}^c_{a/b}$	The column matrix representation of the vector x which belongs to the center point of the frame a with respect to the center point of the frame b and it is resolved in frame c. $\bar{x}^c_{a/b}$ column matrix contains three elements.		

Table 2-1: Notation symbols and definitions

2.2 Extended Kalman Filter Structure and System Model

In this paper, standard fifteen error states Extended Kalman Filter (EKF) structure is implemented with some additional modification. The standard system model for error state Kalman Filter can be found in various resources such as [3], [4] and [5]. The standard form of fifteen error states system model is composed of geographic position error, velocity error, attitude error, accelerometer and gyroscope triad's bias error states. Details of the mathematical model given below can be found extensively in the aforementioned references.

$$\dot{\delta x} = F\delta x + Gw \quad (1)$$

$$\delta x = \left[\underbrace{\delta\bar{r}^{n\ T}_{b/e}}_{1x3}\ \underbrace{\delta\bar{v}^{n\ T}_{b/e}}_{1x3}\ \underbrace{\delta\bar{\psi}^{n\ T}_{b/n}}_{1x3}\ \underbrace{\bar{b}^{b\ T}_{a}}_{1x3}\ \underbrace{\bar{b}^{b\ T}_{g}}_{1x3}\right]^T_{1x15} \quad (2)$$

$$F = \begin{bmatrix} F_{pp} & F_{pv} & 0_{3x3} & 0_{3x3} & 0_{3x3} \\ F_{vp} & F_{vv} & F_{v\psi} & C^n_b & 0_{3x3} \\ F_{\psi p} & F_{\psi v} & F_{\psi\psi} & 0_{3x3} & C^n_b \\ 0_{3x3} & 0_{3x3} & 0_{3x3} & 0_{3x3} & 0_{3x3} \\ 0_{3x3} & 0_{3x3} & 0_{3x3} & 0_{3x3} & 0_{3x3} \end{bmatrix} \quad (3)$$

$$G = \begin{bmatrix} 0_{3x3} & 0_{3x3} & 0_{3x3} & 0_{3x3} \\ C^n_b & 0_{3x3} & 0_{3x3} & 0_{3x3} \\ 0_{3x3} & C^n_b & 0_{3x3} & 0_{3x3} \\ 0_{3x3} & 0_{3x3} & I_{3x3} & 0_{3x3} \\ 0_{3x3} & 0_{3x3} & 0_{3x3} & I_{3x3} \end{bmatrix} \quad (4)$$

$$w=\left[\underbrace{\bar{w}_a^{b\,T}}_{1x3}\ \underbrace{\bar{w}_g^{b\,T}}_{1x3}\ \underbrace{\bar{w}_{b_a}^{b\,T}}_{1x3}\ \underbrace{\bar{w}_{b_g}^{b\,T}}_{1x3}\right]^T_{1x12} \quad (5)$$

where,

$\delta\bar{r}^n_{b/e}$: Geographic position error of the body frame in latitude, longitude and altitude form.

$\delta\bar{v}^n_{b/e}$: Velocity error of the body frame with north, east and down components.

$\delta\bar{\psi}^n_{b/n}$: Attitude error of the body frame with respect to the local navigation frame resolved in the local navigation frame.

$\bar{b}_a$: Bias error of accelerometer triad with x, y and z body axis components.

$\bar{b}_g$: Bias error of gyroscope triad with x, y and z body axis components.

$\bar{w}^b_a$: Velocity random walk noise parameter of accelerometer triad with x, y and z body axis components.

$\bar{w}^b_g$: Angular random walk noise parameter of gyroscope triad with x, y and z body axis components.

$\bar{w}^b_{b_a}$: Bias instability noise parameter of accelerometer triad with x, y and z body axis components.

$\bar{w}^b_{b_g}$: Bias instability noise parameter of gyroscope triad with x, y and z body axis components.

The well-known formulation represented from (1) to (5) is extended with additional five states representing pitch/yaw boresight misalignment angles between platform to body frame and three lever-arm distances between platform to body frame. The additional states can be mathematically modelled as random constant or combination of random constant and random walk with relatively small amplitude. The mentioned mathematical models and the corresponding details can be found in [6]. Theoretically, boresight angles and lever-arm distances between platform and body frame are fixed due to rigid connections. However, in practice, there might be small variations during motion due to vehicle loading conditions, temperature changes etc. Therefore, small amount of modelled system noise definitely increases the robustness of the Kalman Filter estimation of the modelled states for tracking any changes in the true counterpart.

$$\delta x_m = F_m \delta x_m + G_m w_m \quad (6)$$

$$\delta x_m=\left[\underbrace{\delta x^T}_{1x15}\ \underbrace{\delta\psi^{p\,T}_{b/p}}_{1x2}\ \underbrace{\delta\bar{r}^{p\,T}_{b/p}}_{1x3}\right]^T_{1x20} \quad (7)$$

$$w_m=\left[\underbrace{w^T}_{1x12}\ \underbrace{w^{p\,T}_{\delta\psi^p_{b/p}}}_{1x2}\ \underbrace{\bar{w}^{p\,T}_{\delta\bar{r}^p_{b/p}}}_{1x3}\right]^T_{1x17} \quad (8)$$

$$F_m=\begin{bmatrix} F & 0_{15x5} \\ 0_{5x15} & 0_{5x5}\end{bmatrix},\ G_m=\begin{bmatrix} G & 0_{15x2} & 0_{15x3} \\ 0_{2x12} & I_{2x2} & 0_{2x3} \\ 0_{3x12} & 0_{3x2} & I_{3x3}\end{bmatrix} \quad (9)$$

where,

$\delta\psi^p_{b/p}$: Boresight misalignment angles between body and platform frame in Euler pitch and yaw angles form.

$\delta r^p_{b/p}$: Lever-arm distance from the center of platform to the center of body frame with x, y and z platform axis components.

$w^p_{\delta\psi^p_{b/p}}$: Modelled system noise parameter for accounting for the variation in boresight misalignment angles between body and platform frame in Euler pitch and yaw angles form.

$\bar{w}^p_{\delta r^p_{b/p}}$: Modelled system noise parameter for accounting for the variation in lever-arm distance from the center of platform to the center of body frame with x, y and z platform axis components.

The δx_m notation is replaced with δx for the rest of the paper just for preserving simplicity. The well-known predictor and corrector type of EKF algorithm formulation [4], [7] is given between (10) and (14). Since there are different types of measurement models, they are used if their validity control check is satisfied. In case of multiple measurements are allowed in the same time instance, sequential measurement update is implemented.

$$\delta\hat{x}^-_{k+1} = \phi_k \delta\hat{x}^-_k \quad (10)$$

$$P^-_{k+1} = \phi_k P^-_k \phi^T_k + G_k Q_k G^T_k \quad (11)$$

$$K_{k+1} = P^-_{k+1} H^T \left(H P^-_{k+1} H^T + R\right)^{-1} \quad (12)$$

$$\delta\hat{x}^+_{k+1} = \delta\hat{x}^-_{k+1} + K_{k+1}(\delta z_{k+1} - H\delta\hat{x}^-_{k+1}) \quad (13)$$

$$P^+_{k+1} = P^-_{k+1} - K_{k+1} H P^-_{k+1} \quad (14)$$

The equations ranging from (10) to (12) form the time update part of the EKF whereas (13) and (14) form the measurement update part.

2.3 Measurement Models

Extended Kalman Filter measurement models are composed of three different models which are named as ZUPT, ZARUPT and NHCs. They are all applicable for land inertial navigation system without any external hardware requirement or sensor systems other than IMU. For land vehicle applications, the platform stops frequently especially in urban environment. Therefore, if the stationary state of the platform is detected, hypothetical zero velocity and zero angular rate information can be exploited by Kalman Filter. Since movement of land platforms is constrained, NHCs measurements can be used as velocity information while the platform is in motion.

2.3.1 Non-Holonomic Constraints Measurement Model

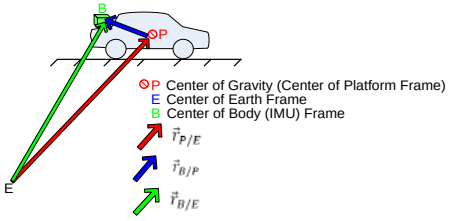

Figure 2-2: Position vector sketch

The position vector pointing the center of platform frame can be written in the following form.

$$\vec{r}_{p/e} = \vec{r}_{b/e} - \vec{r}_{b/p} \quad (15)$$

$$D_n\{\vec{r}_{p/e}\} = D_n\{\vec{r}_{b/e} - \vec{r}_{b/p}\} \quad (16)$$

$$D_n\{\vec{r}_{p/e}\} = D_n\{\vec{r}_{b/e}\} - \left[D_b\{\vec{r}_{b/p}\} + \underbrace{\vec{\omega}_{b/n} \times \vec{r}_{b/p}}_{\text{Cross product}} \right] \quad (17)$$

When expression (17) above is resolved in local navigation frame, expression (18) is found.

$$\bar{v}^n_{p/e} = \bar{v}^n_{b/e} - C^n_b\{\dot{r}^b_{b/p} + ssm(\omega^b_{b/n})\bar{r}^b_{b/p}\} \quad (18)$$

$\dot{r}^b_{b/p}$ term is representing the time derivative of the lever-arm distance between body and platform frame. Since inertial measurement unit is rigidly bolted to the platform, the lever-arm variation can be simply neglected.

$$\bar{v}^n_{p/e} = \bar{v}^n_{b/e} - C^n_b ssm(\bar{\omega}^b_{b/n})\bar{r}^b_{b/p} \quad (19)$$

$$\bar{v}^p_{p/e} = C^p_b C^{nT}_b \bar{v}^n_{b/e} - C^p_b ssm(\bar{\omega}^b_{b/n}) C^{pT}_b \bar{r}^p_{b/p} \quad (20)$$

By multiplying both sides of (19) with $C^p_b C^{nT}_b$ rotation matrices and by simple modification, the velocity relation resolved in platform frame can be found as given in (20). In order to form velocity measurement for error-state Extended Kalman Filter, INS indicated velocity information can be written in the following perturbed error model. The tilde notation "$\tilde{x}$" represents the approximate value of the represented quantity. In other words, the variables with tilde notation contain both true quantity and small error perturbation.

$$\tilde{\bar{v}}^p_{p/e} = \tilde{C}^p_b \tilde{C}^{nT}_b \tilde{\bar{v}}^n_{b/e} - \tilde{C}^p_b ssm(\tilde{\bar{\omega}}^b_{b/n}) \tilde{C}^{pT}_b \tilde{\bar{r}}^p_{b/p} \quad (21)$$

$$\tilde{C}^n_b = (I_{3x3} + ssm(\delta\bar{\psi}^n_{b/n}))C^n_b \ , \ \tilde{C}^p_b = (I_{3x3} + ssm(\delta\bar{\psi}^p_{b/p}))C^p_b \quad (22)$$

Where, $\tilde{\bar{x}} = \bar{x} + \delta\bar{x}$

Since the lever-arm distance is naturally small, the observability of the tactical to navigation grade gyro measurement errors is very weak. Thus, the error term related to gyroscope measurements is ignored. Neglecting high order error terms containing multiplication of two or more error states lead the following expression.

$$\tilde{\bar{v}}^{p}_{p/e}=C^{p}_{b}C^{n^T}_{b}\bar{v}^{n}_{b/e}+C^{p}_{b}C^{n^T}_{b}\delta\bar{v}^{n}_{b/e}+ssm(\delta\bar{\psi}^{p}_{b/p})C^{p}_{b}C^{n^T}_{b}\bar{v}^{n}_{b/e}- \quad (23)$$

$$C^{p}_{b}C^{n^T}_{b}ssm(\delta\bar{\psi}^{n}_{b/n})\bar{v}^{n}_{b/e}-C^{p}_{b}ssm(\bar{\omega}^{b}_{b/n})C^{p^T}_{b}\bar{r}^{p}_{b/p}-C^{p}_{b}ssm(\bar{\omega}^{b}_{b/n})C^{p^T}_{b}\delta\bar{r}^{p}_{b/p}$$

Non-holonomic constraints exploit the fact that the land vehicle generally moves in the forward direction and the motion in the lateral and vertical direction is uncommon. Therefore, vehicle velocity in the platform lateral and vertical direction can be approximated as zero. The measurement model for this type of hypothetical velocity information is given below.

$$z_{NHCs}=\bar{v}^{p}_{p/e}(2,3)+\eta_{\bar{v}^{p}_{p/e}(2,3)}=\begin{bmatrix}\cdots\\ 0+\eta_{\bar{v}^{p}_{p/e}(2)}\\ 0+\eta_{\bar{v}^{p}_{p/e}(3)}\end{bmatrix} \quad (24) \qquad \delta z=z_{NHCs}-\tilde{z} \text{ where, } \tilde{z}=\tilde{\bar{v}}^{p}_{p/e}(2,3) \quad (25)$$

For error state EKF structure, the expression (25) is used as a measurement model. Substituting (23) into the equation (25) lead the Kalman Filter measurement model.

$$\Delta z^{*}=-C^{p}_{b}C^{n^T}_{b}\delta\bar{v}^{n}_{b/e}+ssm(\bar{v}^{p}_{b/e})\delta\bar{\psi}^{p}_{b/p}-C^{p}_{b}C^{n^T}_{b}ssm(\bar{v}^{n}_{b/e})\delta\bar{\psi}^{n}_{b/n}+C^{p}_{b}ssm(\bar{\omega}^{b}_{b/n})C^{p^T}_{b}\delta\bar{r}^{p}_{b/p}+\eta_{\bar{v}^{p}_{p/e}} \quad (26) \qquad \delta z^{*}=H^{*}\delta x+\eta \quad (27)$$

$$H^{*}_{3x20}=\begin{bmatrix}0_{3x3} & -C^{p}_{b}C^{n^T}_{b} & -C^{p}_{b}C^{n^T}_{b}ssm(\bar{v}^{n}_{b/e}) & 0_{3x3} & \cdots\\ 0_{3x3} & A^{*} & C^{p}_{b}ssm(\bar{\omega}^{b}_{b/n})C^{p^T}_{b} & & \end{bmatrix} \quad (28) \qquad \text{Where, } A^{*}=\begin{bmatrix}0 & 0\\ 0 & -\bar{v}^{p}_{p/e}(1)\\ \bar{v}^{p}_{p/e}(1) & 0\end{bmatrix} \quad (29)$$

Since only two out of three velocity components are exploited in measurement model, the Kalman Filter measurement model reduces as follow.

$$\delta z=\delta z^{*}(2,3) \quad H=H^{*}(2:3,:) \quad \eta=\eta^{*}(2,3) \quad (30)$$

For NHC measurement expression, only second and third elements of the matrix are used. Thus, the first element is always discarded and shown in the equations with "…" notation. The expression (26) leads several important outcomes about the observability of the states that can be estimated via NHCs measurements. Due to the fact that detailed observability analysis is out of scope of this study, only the straightforward outcomes of (26) are directly used for making comments. If the expression (26) is examined carefully, the roll misalignment angle between platform and body frame is not observable from non-holonomic constraint measurement whereas the entire three components of the lever-arm distance between platform and body frame is observable. Last but not least, the inertial navigation system indicated three dimensional attitude errors and boresight misalignments angles are not individually and fully observable from non-holonomic constraint measurements. The aforementioned measurement expression indicates that if two types of attitude error states are resolved in platform frame; their differences are observable when NHC measurement concept is utilized. Therefore, it is important that if one of the attitude error uncertainties is small compared to the other type, by exploiting NHC measurements Kalman Filter can accurately estimate the state with high variance. For practical land navigation application, before exploiting NHC measurements on the move, the attitude errors between body to local navigation frame can be successfully reduced using either ZUPT & ZARUPT or navigation aiding systems (e.g. GNSS receiver).

2.3.2 Zero Velocity and Zero Angular Rate Update Measurement Models

When the land vehicle is in stationary condition, zero velocity and zero angular rate information can be used to aid inertial navigation system. The measurement model for this type of hypothetical zero velocity information is given below.

$$z_{ZUPT}=\underbrace{\bar{v}^n_{b/n}}_{0_{3x1}}+\bar{\eta}_{\bar{v}^n_{b/n}}=\bar{\eta}_{\bar{v}^n_{b/n}} \tag{31}$$

For error state EKF structure, the following measurement model is used:

$$\delta z=z_{ZUPT}-\tilde{z} \text{ where } \tilde{z}=\tilde{\bar{v}}^n_{b/n}=(\underbrace{\bar{v}^n_{b/n}}_{0_{3x1}}+\delta\bar{v}^n_{b/n}) \tag{32}$$

$$\delta z=\bar{\eta}_{\bar{v}^n_{b/n}}-\delta\bar{v}^n_{b/n}=H\delta x+\eta \ , \ \eta=\bar{\eta}_{\bar{v}^n_{b/n}} \tag{33}$$

$$H_{3x20}=[0_{3x3} \quad -I_{3x3} \quad 0_{3x3} \quad 0_{3x3} \quad 0_{3x3} \quad 0_{3x2} \quad 0_{3x3}] \tag{34}$$

The measurement model for hypothetical zero angular rate information is given below.

$$z_{ZARUPT}=\underbrace{\bar{\omega}^n_{b/e}}_{0_{3x1}}+\bar{\eta}_{\bar{\omega}^n_{b/e}}=\bar{\eta}_{\bar{\omega}^n_{b/e}} \tag{35}$$

For error state EKF structure, the following measurement model is used:

$$\delta z=z_{ZARUPT}-\tilde{z} \tag{36}$$

$$\text{Where, } \tilde{z}=\tilde{\bar{\omega}}^n_{b/e}=\tilde{C}^n_b\tilde{\bar{\omega}}^b_{b/i}-\tilde{\bar{\omega}}^n_{e/i} \tag{37}$$

$$\tilde{\bar{\omega}}^b_{b/i}=\bar{\omega}^b_{b/i}+\delta\bar{\omega}^b_{b/i} \ , \ \tilde{\bar{\omega}}^n_{e/i}=\bar{\omega}^n_{e/i}+\delta\bar{\omega}^n_{e/i}$$

Term "$\delta\bar{\omega}^b_{b/i}$" represents the error in the gyroscope triad readings and for stationary condition only bias type and noise type error terms are dominant. Thus, $\delta\bar{\omega}^b_{b/i}=\bar{b}^b_g+\bar{w}^b_g$ and term "$\delta\bar{\omega}^n_{e/i}$" can be directly written in terms of latitude error that is $\delta\bar{\omega}^n_{e/i}=-\Omega_{e/i}\begin{bmatrix}\sin(L_{b/e})\\0\\\cos(L_{b/e})\end{bmatrix}\delta L_{b/e}$ [4] where $\delta L_{b/e}=\delta\bar{r}^n_{b/e}(1)$ and $\Omega_{e/i}$= magnitude of the Earth rate. Substituting the above expressions, (22), (37) into (36) and neglecting high order error terms while preserving only first orders yields:

$$\delta z=\text{ssm}(\underbrace{\bar{\omega}^n_{b/i}}_{\bar{\omega}^n_{e/i}})\delta\bar{\psi}^n_{b/n}-C^n_b\bar{b}^b_g-C^n_b\bar{w}^b_g+\delta\bar{\omega}^n_{e/i}+\bar{\eta}_{\bar{\omega}^n_{b/e}}=H\delta x+\eta \tag{38}$$

$$H_{3x20}=\left[\begin{bmatrix}-\Omega_{e/i}\sin(L_{b/e}) & 0 & 0\\0 & 0 & 0\\-\Omega_{e/i}\cos(L_{b/e}) & 0 & 0\end{bmatrix} \quad 0_{3x3} \quad \text{ssm}(\bar{\omega}^n_{e/i}) \quad \ldots\right.$$

$$\left. 0_{3x3} \quad -C^n_b \quad 0_{3x2} \quad 0_{3x3}\right] \ , \ \eta=\bar{\eta}_{\bar{\omega}^n_{b/e}}-C^n_b\bar{w}^b_g \tag{39}$$

The above expression indicates that, accuracy and the integrity of zero angular rate measurement are directly linked to gyroscope triad output noise level. Both practical and theoretical analysis concludes that if there is not any major vibration like disturbances from the host platform, the noise level of the gyroscope is the limiting factor for the accuracy that can be reached with utilizing zero angular rate measurement. For practical applications, it is quite beneficial to reduce the output noise of the gyroscope readings by simple time averaging or zero angular rate measurement implementation can be replaced by integrated zero angular rate measurement model. In this study, moving time average of gyroscope measurements is used to suppress the noise effect. The INS indicated angular rate measurement is replaced with the following expression.

$$\tilde{z}=\tilde{\bar{\omega}}^n_{b/e}=\tilde{C}^n_b\left(\frac{1}{N}\sum_{k=1}^{N}\tilde{\bar{\omega}}^b_{b/i,k}\right)-\tilde{\bar{\omega}}^n_{e/i} \tag{40}$$

3.0 ROBUST ESTIMATOR

For the Kalman Filtering application which relies on mainly inertial navigation, the reliability of any external measurement is quite significant. If the external measurements constitute of hypothetical measurements like ZUPT, ZARUPT and NHCs, availability of the mentioned measurements have to be validated before being exploited as a measurement to the Kalman Filter. Otherwise, if the kinematic quantities do not reflect the actual physical states of the platform, the wrong usage of the measurements try to make the filter estimation non-optimal and even filter stability can be lost. Therefore, in order to preserve the stability, robustness of the filter and the accuracy, precautions have to be taken. For this purpose, two different groups of functions that are responsible for measurement integrity have been implemented.

3.1 Measurement Validity Control

As the name implies it is significant to confirm that the measurement has to be compatible with the actual physical condition. The most straightforward example is the static condition of the vehicle. If the vehicle is in static conditions, the hypothetical measurement of ZUPT is indeed very powerful aiding mechanism for pure land inertial navigation system. However, the exact detection of stationary condition may not be straightforward. In literature, there are many good studies ([8], [9], [10]) which are carried out for stationarity detection task. In this study, the gyroscope based method [8] in simple form is used in combination with basic but powerful INS based detection methodologies. Apart from gyroscopes, there are accelerometer based static detection methods used in several studies [11], [12]. However, mean quadratic deviation or moving average signal of accelerometer based methods practically is not as powerful as gyro based stationary detection logic. Therefore, gyroscope based method is selected as the first part of stationarity detection logic instead of accelerometer based methodologies.

3.1.1 ZUPT and ZARUPT Measurements Validity

In this study, three different motion detection methods are discussed and used simultaneously for static detection.

3.1.1.1 Gyroscope Based Stationarity Detection

When the land platform is in ideal static condition without any vibrational environment, the only sensible rotation rate other than gyroscope sensor errors is the Earth rate and it is very weak signal when compared to the actual motion profile of the land vehicle and the environmental disturbing effects like engine vibration, road irregularities and etc. Therefore, the deviation from the mean value of the gyroscope output signal is very powerful signal for motion detection [8]. For moderate to abrupt motion changes, the gyroscope triad data can be very efficiently used to detect and identify whether the platform in motion or not. In practical application field, gyroscope data should be averaged out for narrow time window or it should be filtered by a simple low pass filter to account for the high frequency noise like disturbances induced from the engine of the vehicle. Simple time average methodology is given below.

$$\bar{\mu}_{gyro} = \frac{1}{N}\sum_{k=1}^{N} \tilde{\omega}^{b}_{b/i,k} \qquad (41)$$

$$\text{Static condition: } \bar{\mu}_{gyro} \leq \xi_{gyro} \qquad (42)$$

ξ_{gyro} is the empirically detected threshold while $\bar{\mu}_{gyro}$ represents the moving average of gyroscope triad data.

3.1.1.2 INS Speed Based Stationarity Detection

The stationarity condition of the vehicle can be detected for the most majority of the mission time via the usage of speed information which can be obtained from the velocity output of the readily available INS. If there is a

built-in Kalman Filter accompanying to INS, then the speed uncertainty information can be obtained from state covariance matrix which is then used for the application of speed based stationarity condition.

$$|\tilde{\bar{v}}^n_{b/e}| = \underbrace{|\bar{v}^n_{b/e}|}_{0 \text{ if static}} + |\delta\bar{v}^n_{b/e}| = |\delta\bar{v}^n_{b/e}| \quad \text{Static condition:} \quad |\delta\bar{v}^n_{b/e}| \leq \xi_{speed}\sigma_{|\delta\bar{v}^n_{b/e}|} \tag{43}$$

$$\text{with } \sigma_{|\delta\bar{v}^n_{b/e}|} = \sqrt{P_{\bar{v}^n_{b/e}(1)} + P_{\bar{v}^n_{b/e}(2)} + P_{\bar{v}^n_{b/e}(3)}}$$

$\sigma_{|\delta\bar{v}^n_{b/e}|}$ is standard deviation of the expected speed error and $P_{\bar{v}^n_{b/e}(i)}$ is velocity related diagonal elements of the state covariance matrix. ξ_{speed} is representing the confidence level of error statistics and it is taken as 2 for %95 confidence.

Since the method mentioned above creates direct link between physical condition and Kalman Filter estimation statistics, performance level of IMU sensors and available navigation aids is quite important. The worst case scenario is the pure inertial navigation without any aiding after initialization. To illustrate the effectiveness of this methodology, the covariance analysis for pure INS is carried out for typical land vehicle mission scenario with two different grades of IMU. The performance parameters of IMUs that are used in this analysis are given in Table 3-1.

	Error Parameter	Low Noise Tactical Grade IMU	Navigation Grade IMU
Accelerometer	Input Range	± 10 g	± 10 g
	Bias	1.0 mg	0.05 mg
	Scale Factor	150 ppm	50 ppm
	Axis Misalignment	1 mrad	0.1 mrad
	Velocity Random Walk (VRW)	50 μg/$\sqrt{Hz}$	5 μg/$\sqrt{Hz}$
Gyroscope	Input Range	± 500 °/sec	± 500 °/sec
	Rate Bias	1.0 °/hr	0.05 °/hr
	Rate Scale Factor	150 ppm	50 ppm
	Axis Misalignment	1 mrad	0.1 mrad
	Angular Random Walk (ARW)	0.015 °/$\sqrt{hr}$	0.005 °/$\sqrt{hr}$

Table 3-1: Simulated IMU performance parameters

As it can be clearly inferred from the Figure 3-1, if the platform does not undergo creeping like very low speed motion, speed based method can be effectively used when INS is built with especially navigation grade IMU.

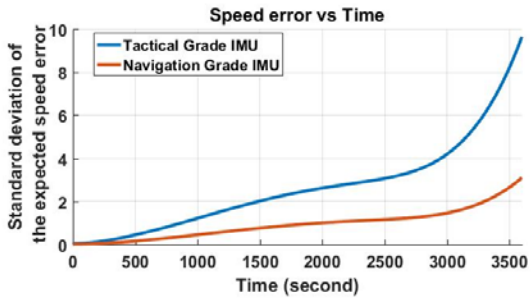

Figure 3-1: Standard deviation of the expected speed error

3.1.1.3 Navigation Frame Acceleration Based Stationarity Detection

The acceleration in navigation frame can be written in the following form [4].

$$\bar{a}^n_{b/e} = \bar{f}^n_{b/i} + \bar{g}^n_b - (\text{ssm}(\bar{\omega}^n_{n/e}) + 2\text{ssm}(\bar{\omega}^n_{e/i}))\bar{v}^n_{b/e} \tag{44}$$

$$\text{Static condition:} \quad |\bar{a}^n_{b/e}| \leq \xi_{\bar{a}^n_{b/e}} \tag{45}$$

$\xi_{\bar{a}^n_{b/e}}$ is empirically detected acceleration threshold. The expression given in (45) satisfies when the vehicle in stationary condition or constant velocity cruise condition. The empirical results obtained from field tests carried out with land vehicle indicate that gyroscope based and navigation frame acceleration based methods are highly effective at motion detection when the platform undergoes abrupt motion changes. When the platform moves on good road surfaces with low level of dynamics, speed based method effectively overwhelm the other methods. Therefore, speed based method can be combined together with gyroscope based and/or navigation frame acceleration based methods in a complementary manner.

3.1.2 NHCs Measurements Validity

The constrained motion assumption for land platforms state that the center of vehicle platform frame has only one non-zero velocity component which is in the forward direction. This assumption is valid for the most majority of the mission profile of the land vehicle. However, when the vehicle undergoes sharp maneuvers there is a possibility to violate the mentioned assumption with lateral and vertical velocity component in platform frame. Therefore, gyroscope based and navigation frame acceleration based methods given in stationary detection part can be combined together with different empirically detected threshold values to enable the usage of NHCs measurements. The thresholds should be compatible with the vehicle handling characteristics and the road conditions.

3.2 Adaptive Innovation Filtering

The designed EKF is modified such a way that adaptive gain control for the Kalman gain calculation is carried out with measurement innovation based methodology. The robust maximum likelihood estimation (M-estimate) [13] is applied to the Kalman Filter with the equivalent weight based on bifactor reduction [14]. M-estimator based adaptive Kalman gain control is efficient way of controlling the Kalman Filter response to the measurements especially when there is mismatch between the measurements and the physical condition that it corresponds to or measurement containing erroneously large error. Moreover, this innovation based structure preserves the integrity of the measurements and thus the filter.

$$\delta z' = \delta z - H\delta x \quad , \quad \sigma_{\delta z'} = \sqrt{\left(HPH^T + R\right)} \quad , \quad \mu_{\delta z'} = \frac{\delta z'}{\sigma_{\delta z'}} \tag{46}$$

$$K_{eq} = K \begin{cases} 1 & |\mu_{\delta z'}| \le c_0 \\ \dfrac{c_0}{|\mu_{\delta z'}|}\dfrac{(c_1 - \mu_{\delta z'})}{(c_1 - c_0)} & c_0 < |\mu_{\delta z'}| \le c_1 \\ 0 & c_1 < |\mu_{\delta z'}| \end{cases} \tag{47}$$

$\mu_{\delta z'}$ is normalized innovation which has been normalized with the innovation covariance and K_{eq} is equivalent Kalman gain scaled with measurement innovation statistics. c_0 and c_1 represent integer constants and they are selected as $c_1 = 6c_0 = 6$ which corresponds six sigma error statistics.

4.0 SIMULATION STUDY

Simulation study is mainly composed of covariance analysis and Monte-Carlo analysis which is essential part of statistical analysis and it is heavily depend on multi simulation runs. The formulation, derivation and the algorithm structure of the aforementioned analysis methods are not discussed here due to their well-known description given in [15], [16].

This part of the paper targets two fundamental performance analyses. First one is an azimuth accuracy level that can be achievable with ZUPT and ZARUPT measurements. Second aim is to carry out performance analysis related to the combination of all of the hypothetical measurements applied to the land vehicle mission scenario whereas the effect of NHCs measurements on navigation positioning performance is the primary concern.

4.1 Azimuth Accuracy Analysis

Azimuthal error is the one of the most significant error source other than ones owned by inertial sensors when the accuracy level of the pure inertial system is concerned. If there are not any available navigation aiding systems or external azimuth information, the classical way of initial azimuth detection is based on gyro compassing technique. The gyro compassing is a one of the fundamental way of azimuth detection via measurement of the components of the Earth rate with the gyroscope triad. Since the methodology requires accurate gyroscopes to sense the Earth rate, deterministic and stochastic errors of gyroscopes play very significant role in azimuth angle detection of INS. The azimuth accuracy that can be achievable with the gyro compassing method [17] can be represented in the following form.

$$\sigma^2_{\text{gyrocompass}}\,(\text{rad}) = \sigma^2_{\text{acc\_bias}}(\text{g}) + \frac{\sigma^2_{\text{gyro\_bias}}(^\circ/\text{hr})}{|\Omega_{\text{e/i}}(^\circ/\text{hr})|\cos^2(\text{L}_\text{b})} \qquad (48)$$

In the above expression the effect of measurement noise of gyros are simple discarded and bias type error in gyroscope measurements is the major error source for azimuth accuracy that can be obtainable with gyro compassing. If the platform that IMU is strapped to can be rotated in local vertical direction, the effect of bias type error can be reduced by estimating the bias error of gyros and the azimuthal angle error simultaneously. The covariance analysis is carried out in this section for attainable theoretical azimuthal accuracy gain. The simulation starts with gyro compassing process for stationary platform and later simple rotational trajectory around local vertical axis is followed. The analysis is carried out with ZUPT and ZARUPT aiding option individually for IMUs whose error parameters are given in the Table 3-1. Although the effects of the missing error parameters that are not modelled in the Kalman Filter structure given in Chapter 2 are weak for this simple trajectory and objective, the Kalman Filter model given in Chapter 2 is used with the additional error states for completeness of the analysis. The additional sensor error parameters can be included into Kalman filter with random constant models and details can be found in [18]. The simulation is repeated with varying the measurement noises of ZUPT and ZARUPT aiding. The following figure indicates the theoretical azimuthal uncertainty level that can be achievable within the modelled ideal simulation environment.

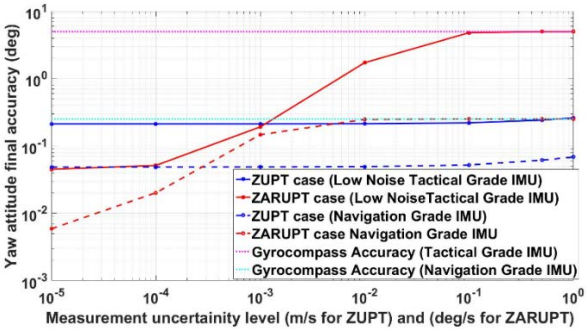

Figure 4-1: Yaw/Azimuth attitude theoretical accuracy for low noise tactical grade and navigation grade IMU

The Figure 4-1 shows that ZARUPT aiding outperforms ZUPT aiding in terms of azimuthal accuracy. This conclusion is valid for very low level of angular rate measurement noise. However, it can be deduced from (39) that zero angular rate error measurement contains both gyroscope output noise and the external vibration like disturbances that are affecting the IMU. Therefore, the accuracy level that can be obtainable from ZARUPT aiding is limited with both gyroscope output noise and environmental physical disturbances. In practical quasi-static environment where there is no engine vibration, wind and etc. it can be approximated that the azimuthal accuracy with ZARUPT aiding is limited with the angular random walk parameter of the gyroscopes. In order to reduce the effect of the output noise which mainly in the form of white noise, one can use simple noise suppression techniques like moving time average to improve and reach the higher

performance presented in Figure 4-1. On the other hand, if the noise level of the gyroscopes is relatively high, ZUPT aiding should be selected over ZARUPT.

4.2 Horizontal Positioning Accuracy Analysis

The horizontal positioning analysis is carried out with a Monte-Carlo analysis with 200 simulation run where the whole error statistics are attributed as a zero mean Gaussian distribution with a known variance. Simulated trajectories contain very basic heading change and stop type profile named as pre-calibration trajectory which is simply the same profile used in the azimuth accuracy analysis. In the pre-calibration trajectory, the land vehicle is simulated to stop after 90 degrees heading change until the initial azimuth orientation reached. Later on, the land vehicle undergoes a one hour constant speed cruise mission without stopping with a heading change trajectory based on constant heading change rate. Figure 4-2 and Figure 4-3 illustrate eight different simulation trajectories with a distinct and constant heading change rate. The all of the eight trajectories are used with IMU specifications given in Table 3-1 individually for Monte Carlo analysis.

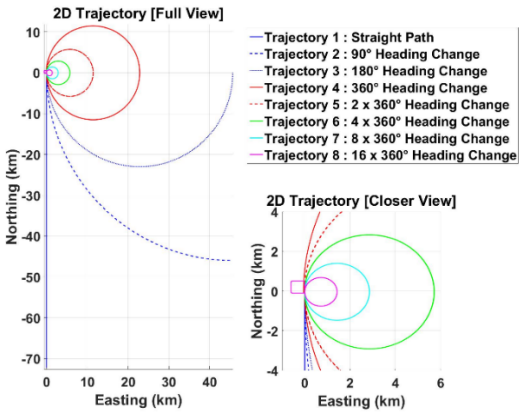

Figure 4-2: Simulated 2D trajectories

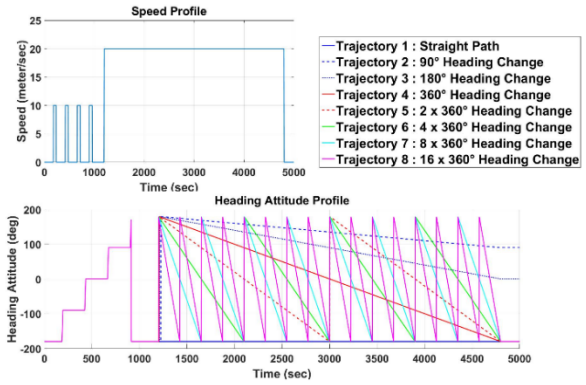

Figure 4-3: Speed and heading profiles of the simulated trajectories

The positioning error curves obtained from each simulation run are stored and 50% Circular Error Probable (CEP) statistic is calculated and presented in Figure 4-4.

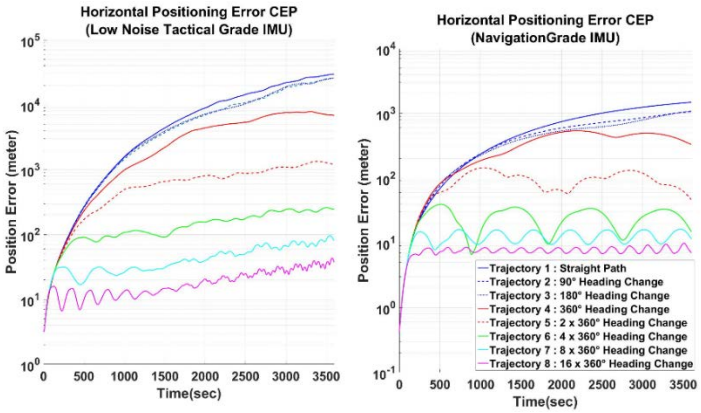

Figure 4-4: Horizontal positioning accuracy of multi-run analysis for low noise tactical grade IMU and navigation grade IMU

Figure 4-4 clearly indicates that the horizontal positioning accuracy is directly related to the heading angle change for both of the IMU types. Additionally, the worst performance equivalent to pure INS performance level is obtained for straight path profile regardless of the IMU specifications. Thus, the positioning performance correlation with heading change is obtained from the simulation studies. The terminal positioning performance obtained in each simulated trajectory for one hour navigation mission is tabulated in the following table. The positioning error is for each trajectory given in both meter and the ratio to Distance Travelled (DT).

Trajectory ID	Horizontal Positioning Error CEP (1 hour mission)	
	Low Noise Tactical Grade IMU	Navigation Grade IMU
Trajectory 1	29720 meter (41.28% DT)	1478 meter (2.06% DT)
Trajectory 2	25864 meter (35.92% DT)	1078 meter (1.50% DT)
Trajectory 3	25453 meter (35.35% DT)	1062 meter (1.48% DT)
Trajectory 4	7845 meter (10.90% DT)	534 meter (0.74% DT)
Trajectory 5	1339 meter (1.86% DT)	144 meter (0.20% DT)
Trajectory 6	257 meter (0.36% DT)	39 meter (0.05% DT)
Trajectory 7	96 meter (0.13% DT)	16 meter (0.02% DT)
Trajectory 8	43 meter (0.06% DT)	10 meter (0.01% DT)

Table 4-1: Horizontal positioning error for statistical simulation analysis

The results given in Table 4-1 are used as a data set for curve fitting and the following exponential shape performance correlation is found.

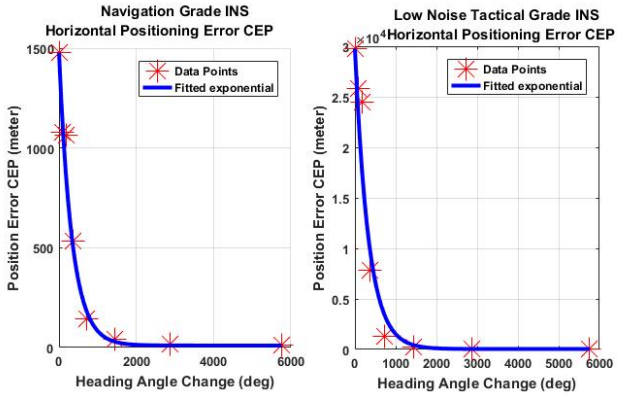

Figure 4-5: Horizontal positioning accuracy vs heading angle change correlation

The fitted expression and the constants are found in the following forms.

$$\delta p(\Delta\psi)=a_0+a_1\exp(a_2\Delta\psi) \qquad (49)$$

Constants	Low Noise Tactical Grade IMU	Navigation Grade IMU
a_0	43 meter	10 meter
a_1	29677 meter	1468 meter
a_2	-0.003 deg $^{-1}$	-0.003 deg $^{-1}$

Table 4-2: Horizontal positioning error regression constants

5.0 EXPERIMENTAL STUDY

Experimental study and field tests are carried out with two commonly known commercialized IMU products called ISA-100C and HG1700. ISA-100C is a Fiber Optic Gyroscope (FOG) based low noise high-end tactical i.e. near-navigation grade IMU developed by the company called Northrop Grumman LITEF. HG1700 is a Ring Laser Gyroscope (RLG) based tactical grade IMU which is very well known product in the commercial market and it is developed by Honeywell.

Figure 5-1: ISA-100C positioned in the left whereas HG1700 IMU is located in the right

	Error Parameter	HG1700	ISA-100C
Accelero-meter	Input Range	± 50 g	± 10 g
	Bias	1.0 mg	1.25 mg
	Scale Factor	300 ppm	100 ppm
	Velocity Random Walk (VRW)	85 µg/$\sqrt{Hz}$	100 µg/$\sqrt{Hz}$
Gyroscope	Input Range	± 1000 °/sec	± 495 °/sec
	Rate Bias	1.0 °/hr	0.2 °/hr*
	Rate Scale Factor	150 ppm	100 ppm
	Angular Random Walk (ARW)	0.125 °/$\sqrt{hr}$	0.012 °/$\sqrt{hr}$
* Tested rms repeatable bias error for the gyroscope triad			

Table 5-1: HG1700 and ISA-100C IMU performance parameters

For the entire test campaign, ISA-100C IMU is integrated with the Novatel Propak-6 GNSS receiver under the name of Sync Positioning and Navigation (SPAN) system developed by the company Novatel. SPAN system is taken as a reference system that supplies the ground truth navigation information. The inertial sensors data from ISA-100C are collected from SPAN system. On the other hand, HG1700 is integrated in modular INS/GNSS integration platform developed by ROKETSAN called as ALBATROS system. Therefore, modified version of ALBATROS system is used for both data collection from HG1700 and algorithm performance trials with a modification done mechanically and electronically.

Figure 5-2: ALBATROS INS/GNSS integrated navigation system located in the right whereas modified version of ALBATROS system for adapting HG1700 IMU is located in the left

Figure 5-3: ALBATROS system and ISA-100C IMU fixed to the common mechanical fixture

The test campaign carried out during in this part begins with a misalignment angle detection test which is necessary for obtaining the misalignment angles between two IMU body axes which are fixed just after they are bolted to the mechanical fixture. The misalignment angles are calculated in three repeated tests and the average values are used in the rest of the test campaign for comparison. The misalignment angle detection is carried out with the calibrated and compensated accelerometer data of both of the IMUs. Since the accelerometer dominant residual errors are calibrated in laboratory environment, the uncertainty in misalignment angle detection calculation is negligible small.

Azimuth accuracy test is carried out in laboratory environment with a simple azimuth change motion profile given in Figure 5-4. Azimuth accuracy test is applied only to algorithm solution utilizing HG1700 IMU due to fact that the ISA-100C IMU integrated SPAN system provides the reference azimuth information in with gyro compassing feature.

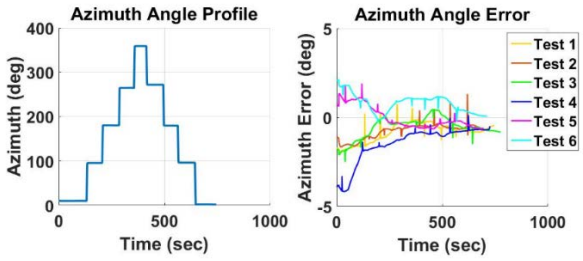

Figure 5-4: Yaw angle profile and error curves for laboratory tests

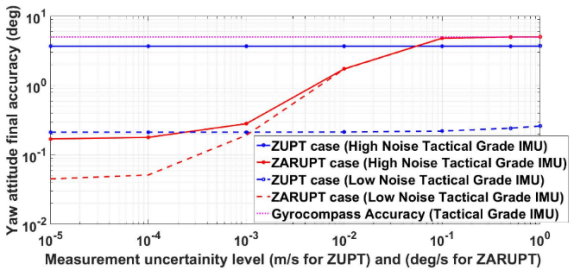

Figure 5-5: Yaw/Azimuth attitude theoretical accuracy for low and high noise tactical grade IMU

Figure 5-4 indicates the results of the azimuth accuracy test which is repeated 6 times and around 0.6 degree rms azimuth accuracy can be achievable with the HG1700 like IMU with ZARUPT aiding. Although the entire simulation analysis for tactical grade IMU is carried on for low gyroscope ARW value, 0.5 - 1 degree azimuth angle accuracy level is an expected value due to the fact that the output noise level of the gyroscope belonging to HG1700 IMU. The output noise is on average around 0.1 degrees/s and this is very high value that is limiting the further accuracy achievable with both ZUPT and ZARUPT aiding. In order to verify the test results obtained from the azimuth accuracy test, the simulation analysis carried out for low noise tactical grade IMU is remade with the increased angular random walk parameter of gyroscopes to simulate HG1700 IMU. The results of the simulation study are presented in Figure 5-5. High noise tactical grade IMU represents HG1700 and Figure 5-5 illustrates that ZUPT aiding cannot provide more than around 3 degree heading accuracy whereas ZARUPT aiding can reduce the azimuth uncertainty below 1 degree if noise suppression techniques are applied to the gyroscope data. Therefore, the experimental azimuth accuracy tests are compatible with the simulation analysis.

In order to verify the positioning accuracy results obtained in simulation analysis, the land vehicle navigation survey test is planned. Both of the IMUs mentioned above are mounted to the land vehicle trunk area with Propak6 GNSS receiver, GNSS antennas and power supplies. Figure 5-6 depicts the instrumented land vehicle.

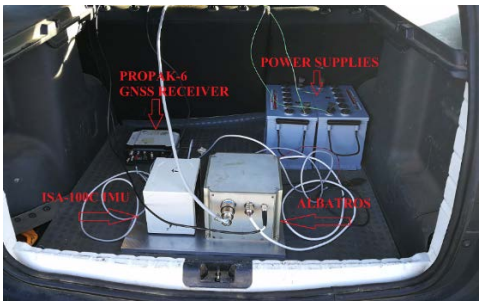

Figure 5-6: View from the instrumented land vehicle

As it is mentioned earlier, inertial sensor data and SPAN system INS/GNSS integrated navigation solutions are continuously collected throughout the entire field test scenarios. Two different IMU sensor data are fed to the developed algorithm which uses ZUPT, ZARUPT and NHCs navigation aiding. Additionally, the designed test trajectory begins with the heading change maneuvers which are very similar to the trajectory profile given in the simulation analysis as pre-calibration trajectory. During pre-calibration trajectory profile, azimuth angle and inertial sensor bias refinements are done with ZUPT and ZARUPT measurements. Later on, the navigation survey phase starts in which the land vehicle does not stop for one hour mission time. The same test procedure is followed five times with varying trajectory, location and speed. For the whole test campaign, GNSS receiver is only activated for obtaining SPAN system integrated navigation solution and detection of initial position information which is necessary for the initialization of the INS mechanization algorithm. The integrated

navigation solution serves as ground-true data sets for forming reference and comparison purposes. Figure 5-7 shows the five distinct trajectories followed during the positioning accuracy test. First two test trajectories consist of constant rotation sequences whereas the last three trajectories follow a long distance range mission.

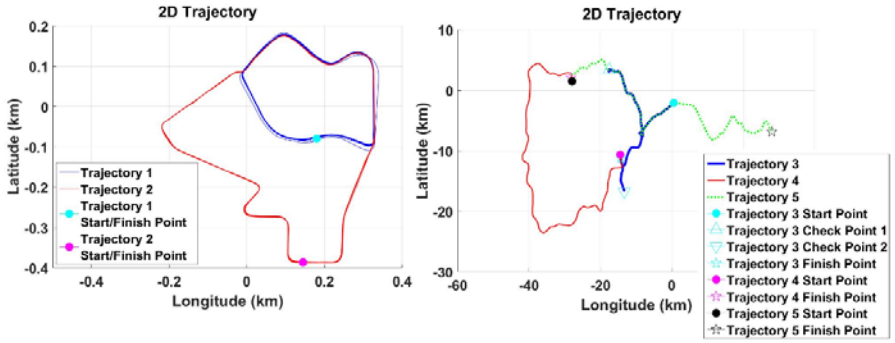

Figure 5-7: Two dimensional trajectory profiles for five distinct field tests

The horizontal positioning accuracy results of the field tests are given in the following figures.

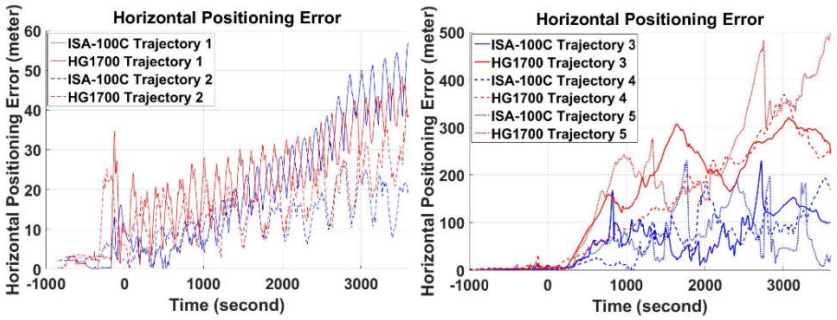

Figure 5-8: Horizontal positioning error for field tests

Figure 5-8 shows that both of the system has a very low error growth rate for the first two trajectories. However, for the last three trajectories, the algorithm solution using ISA-100C IMU data outperforms the one with HG1700 IMU. In order to clearly identify and justify the test results, performance outcomes are tabulated in Table 5-2.

		Field Test No*				
		No1	**No2**	**No3**	**No4**	**No5**
	Travelled Distance (DT)	23.8 km	23.3 km	60.8 km	66.7 km	69.8 km
	Spanned total heading angle	15650°	15865°	4448°	2707°	3020°
IMU ISA-100C	**Horizontal positioning error** (1 hour) [% DT]**	52.5 m (%0.22 DT)	21.7 m (%0.09 DT)	100.1 m (%0.16 DT)	29.5 m (%0.04 DT)	169.4 m (%0.24 DT)
IMU HG 1700	**Horizontal positioning error** (1 hour)**	41.9 m (%0.18 DT)	39.0 m (%0.17 DT)	245.5 m (%0.40 DT)	251.0 m (%0.38 DT)	496.8 m (%0.71 DT)

* Test numbers are compatible with the trajectory numbers. For instance, no1 represents the first trajectory.
** Horizontal positioning error is the final error value taken at the end of 1 hour operation where inertial navigation system is only aided with NHCs measurements

Table 5-2: Navigation survey overall test results

Before interpreting the test results, it should be pointed out that only ISA-100C IMU satisfies the performance specifications given as low noise tactical grade IMU which is used in the simulation analysis. Although HG1700 IMU is considered in tactical grade category, the output noise values of gyroscopes are quite high especially in the dither mechanism axis.

The trajectory profiles followed in the first two tests contain around 4 times more heading angle change and the change rate is nearly homogenously to the full test duration. The positioning performance is similar for the both of the IMU type and in average of 40 meter accuracy can be reached for 1 hour navigation mission. The result obtained from Table 4-2 and Figure 4-5 yield 43 meter CEP type positioning error for more than 5400 degree total heading change during 1 hour mission and the field test results highly match with the simulation work.

The positioning performance obtained for ISA-100C IMU outperforms the one with HG1700 IMU for the last three tests. The major difference between the two different groups of trajectory profiles is the distance travelled and the total azimuth change during the mission. If the total spanned azimuth angle decreases and the platform follow more straight trajectory, the velocity error in the forward direction of the platform develop rapidly depending on the quality of the IMU used. This result is expected and shown both in the simulation analysis and the field tests. The main reason behind is that the NHCs measurement can only provide two out of three components of the velocity vector information. Therefore, the missed velocity component makes the inertial navigation velocity calculation vulnerable to the error in that direction. Additionally, the heading angle change maneuver reduces the impact of inertial sensor error parameters on velocity error growth and the results related to this phenomenon can be seen from the last three field test results. During the last three tests, the total spanned heading angle change is small when compared to the first two tests and the effect of the quality of the inertial sensors can be clearly identified from the positioning accuracy given in Table 5-2. Moreover, if the Table 5-2 is examined carefully, the positioning performance which is more accurate than 0.25% DT can be achievable with ISA-100C IMU whereas 0.75% DT performance level can be obtained with HG1700 type IMU.

6.0 CONCLUSION

In conclusion, this paper targets the attainable performance gain of the pure inertial navigation systems that are aided with the hypothetical measurements applicable for the land vehicle navigation mission. The hypothetical measurements are composed of ZUPT, ZARUPT and NHCs measurements and their effects on the pure inertial navigation system are analysed with simulation and field tests. Before jumping in the simulation analysis and field tests, the methodology followed for improving the robustness of the estimation filter is explained. Since the hypothetical measurements are not supplied from any kind of external hardware, their validity control has to be made sure from the available sources to satisfy the correctness of the assumptions and the physical state of the real platform. In more specific way, static condition instances have to be made sure for using ZUPT and ZARUPT aiding. Therefore, INS based simple but efficient methods are defined and used together with gyro based method for static detection purposes. Moreover, innovation based Kalman filter gain scaling is also implemented to improve the robustness of the estimation filter.

The simulation analysis begins with the azimuth accuracy analysis obtainable with ZUPT & ZARUPT measurements and two different grades of IMU are used throughout the analysis. Simulation results indicate that the gyroscope noise is the fundamental sensor parameters that have a significant impact on the capability of the algorithm to reach higher performance. This conclusion is applicable for both of ZUPT and ZARUPT measurements. However, if the output noise levels of the intended gyroscopes are lower than approximately magnitude of the Earth rate signal, the ZARUPT aiding has a high capability to outperform ZUPT concept. Additionally, the noise in the gyro measurements can be reduced with a low pass filter or simply moving time average techniques to further improve and increase the usability of ZARUPT concept in real application field. The azimuth accuracy analysis is followed by the positioning accuracy analysis carried out in simulation world to analyse the performance gain from NHCs measurements. During the simulation tests, different trajectory profiles are simulated with varying the heading change rate for a 1 hour navigation survey mission. Each of the simulated trajectory profiles are started with around 20 minutes pre-calibration routine for azimuth angle and inertial sensor bias estimation process. The pre-calibration routine can be taken as a fine alignment phase of the commercial inertial navigation systems and during that phase, ZUPT and ZARUPT measurements are exploited with the frequent heading change motion profile. After the pre-calibration routine is done, the

simulated trajectory profiles continue with 1 hour non-stopping navigation survey mission with constant heading change rate. The analysis shows that exponential type of horizontal positioning performance gain which is correlated with the spanned heading angle exists. Therefore, NHCs measurement is shown to be very effective way of aiding the pure inertial navigation system. As long as the land platforms do not follow strictly straight path, the performance gain from NHCs measurements is very promising and full straight path scenario is not a very common trajectory profile.

The field tests carried out in this study result in very supportive outcomes about the validness of the simulation results. During the land vehicle navigation test mission, two different very famous IMU called HG1700 and ISA-100C are used and the performance analysis is carried out with their sensor data. Additionally, the integrated navigation solution of the SPAN system composed of ISA-100C and Propak6 GNSS receiver is collected for the ground true reference data which is necessary for quantifying the results of the algorithm depend on hypothetical measurements. The field test horizontal positioning results indicate that NHCs aiding significantly increase the pure inertial navigation performance of the inertial navigation systems uses both of the aforementioned IMUs individually. As long as the vehicle is changing its heading attitude, less than 0.25% DT horizontal positioning performance is shown to be achieved with an IMU like ISA-100C whereas 0.75% DT performance is achieved with HG1700 IMU. The exponential shape performance improvement function found during the simulation analysis is compatible with the real field tests. Additionally, the field test results indicate that the land platform does not necessarily to follow circular shape trajectory. The only requirement is to have a heading angle change during motion profile and the change is not need to be only in one direction. Therefore, total magnitude of the spanned heading attitude should be taken into consideration.

The horizontal positioning performance level obtained both in the simulation analysis and field tests are very promising when it is compared with the land inertial navigation systems aided with odometer. In this paper, odometer is not considered at all but this device is one of the fundamental sensor that is commonly built-in the land platforms. Moreover, the odometer in its simple form measures the vehicle velocity in forward direction which is the missing velocity information when NHCs aiding is considered. Theoretically the combination of odometer and NHCs is definitely a very promising and further analysis and test campaigns with an odometer addition is left for future work study.

7.0 ACKNOWLEDGMENT

This work was performed with a great support from ROKETSAN in terms of hardware, test environment and facility. Therefore, special thanks are owed to ROKETSAN.

8.0 REFERENCES

[1] P. G. Savage, Strapdown Analytics, 2nd ed., vol.1. Maple Plain, 2000.

[2] R. M. Rogers, Applied Mathematics in Integrated Navigation Systems, 2nd ed., American Institude of Aeronautics and Astronautics, Inc. 2003, pp. 41-90.

[3] D. H. Titterton, and J. L. Weston, Strapdown Inertial Navigation Technology, 2nd ed., The Institution of Electrical Engineers, 2004, pp. 17-55.

[4] P. D. Grooves, Principles of GNSS, Inertial, and Multisensor Integrated Navigation Systems, Artech House, 2008.

[5] A. Noureldin, T. Karamat, and J. Georgy, Fundamentals of Inertial Navigation, Satellite-based Positioning and their Integration, Springer, 2013, pp. 225-270.

[6] M. El-Diasy, and S. Pagiatakis, "Calibration and stochastic modelling of inertial navigation sensor errors," Journal of Global Positioning Systems, vol. 7, 2008, pp. 170-182.

[7] D. Simon, Optimal State Estimation, Wiley Interscience, 2006.

[8] I. Skog, P.Handel, J. L. Nilsson, and J. Rantakokko, "Zero-velocity detection-an algorithm evaluation," Biomedical Engineering, IEEE Transactions on, vol. 57, November 2010, pp. 2657-2666.

[9] A. Ramanandan, A. Chen, and J. A. Farrell, "Inertial navigation aided by stationary updates," Intelligent Transportation Systems, IEEE Transactions on, vol. 13, March 2012, pp. 235-248.

[10] R. Feliz, E. Zalama, and J. G. Garcia-Bermejo, "Pedestrian tracking using inertial sensors," J. Phys. Agents, vol. 3, January 2009, pp. 35-43.

[11] A. Pretto, and G. Grisetti, "Calibration and performance evaluation of low-cost IMUs," 20th IMEKO TC4 International Symposium, September 2014.

[12] A. Zujevs, V. Vecins, and A. Korsunovs, "A method for static and dynamic interval detection within the imu calibration procedure," in press.

[13] Y. Zhao, "Gps/imu integrated system for land vehicle navigation based on mems", Master of Science Thesis, Royal Institue of Technology, September 2011.

[14] Y. Yang, L. Song, and T. Xu, "Robust estimator for correlated observations based on bifactor equivalent weights," Journal of Geodesy, vol. 76, 2002, pp. 353-358.

[15] J. A. Farrell, Aided Navigation, GPS with high rate sensors, McGraw Hill, 2008, pp. 217-233.

[16] R. G. Brown, and P. Y. C. Hwang, Introduction to Random Signals and Applied Kalman Filtering, 3th ed., Wiley, 1985.

[17] M. S. Grewal, A. P. Andrews, and C. G. Bartone, Global Navigation Satellite Systems, Inertial Navigation, and Integration, 3th ed., Wiley, 2013, pp. 84-87.

[18] L. O. Yaman, "Extended kalman filter based muti-purpose inertial sensor field calibration algorithm, Master of Science Thesis, Middle East Technical University, December 2017.